

Variational Umbrella Seeding for Calculating Nucleation Barriers

Willem Gispen,¹ Jorge R. Espinosa,² Eduardo Sanz,² Carlos Vega,² and Marjolein Dijkstra¹

¹*Soft Condensed Matter & Biophysics, Debye Institute for Nanomaterials Science, Utrecht University, Princetonplein 1, 3584 CC Utrecht, Netherlands*

²*Departamento de Química Física, Facultad de Ciencias Químicas, Universidad Complutense de Madrid, 28040 Madrid, Spain*

(*Electronic mail: m.dijkstra@uu.nl)

(Dated: 22 February 2024)

In this work, we introduce Variational Umbrella Seeding, a novel technique for computing nucleation barriers. This new method, a refinement of the original seeding approach, is independent on the choice of order parameter for measuring the size of a nucleus. Consequently, it surpasses seeding in accuracy, and Umbrella Sampling in computational speed. We test the method extensively and demonstrate excellent accuracy for crystal nucleation of nearly hard spheres and of two distinct models of water: mW and TIP4P/ICE. This method can easily be extended to calculate nucleation barriers for homogeneous melting, condensation, and cavitation.

A first-order phase transition from a metastable phase to a more stable phase often occurs through the formation of a nucleus of the new phase. This nucleation process is apparent in phase transitions such as crystallization, melting, condensation, and cavitation. In crystallization, for example, nucleation determines the crystal polymorph and thus the material properties of the crystalline phase. More generally, the time required for the phase transition to start is determined by the nucleation rate. Simulations enable us to gain insight in the nucleation mechanisms and the factors influencing the nucleation rate. This insight can then be used to understand, predict, or even control nucleation in natural and industrial processes.

However, nucleation is a rare event, meaning that nucleation takes a very long time to occur spontaneously in simulations. Except for the simplest model systems, direct measurements of nucleation rates are thus not feasible in simulations. To overcome this rare-event challenge, several enhanced sampling techniques have been introduced, such as forward flux sampling,¹ transition path sampling,² metadynamics,^{3,4} lattice mold,⁵ and Umbrella Sampling.^{6,7} Although these techniques are much faster than brute-force simulations, they still require substantial computational resources. As a consequence, most nucleation studies focus on only a few selected state points.

To gain more insight into nucleation trends, it is useful to combine simulations with classical nucleation theory (CNT).^{8,9} The seeding technique¹⁰ leverages this approach to estimate nucleation rates with much greater efficiency, and across wider ranges of conditions compared to traditional methods. This advancement has allowed the study of the thermodynamics of curved interfaces,¹¹ polymorph selection,¹² and nucleation phase diagrams.^{13,14} Despite its approximate nature, the seeding technique has demonstrated to give accurate results across a wide variety of scenarios such as Lennard-Jones condensation, crystallization of hard spheres, water, and NaCl,^{10,15–17} and melting of hard spheres.¹⁸

However, challenges arise in applying the seeding technique. At its core, this technique relies on CNT approximations for the nucleation rate J and the nucleation barrier ΔG^c ,

given by

$$J = J_0 \exp(-\Delta G_{\text{CNT}}^c / k_B T), \quad (1)$$

$$\Delta G_{\text{CNT}}^c = \frac{1}{2} n_c |\Delta \mu|. \quad (2)$$

Here J_0 denotes the kinetic prefactor, k_B represents Boltzmann's constant, T the temperature, n_c the size of the critical nucleus, and $|\Delta \mu|$ is the supersaturation, i.e. the difference in chemical potential between the solid and liquid phases. From the CNT approximation, Equation (2), it is evident that the nucleation barrier is directly determined by the critical nucleus size n_c . To calculate this size, an order parameter (or criterion) is required to distinguish between the nucleus and the surrounding parent phase. Different order parameter choices yield different nucleus sizes, and consequently, different nucleation barriers. Thus the results of seeding simulations depend on the order parameter choice. In contrast, more rigorous rare-event methods such as Umbrella Sampling and metadynamics have been shown to depend only weakly on the chosen criterion for measuring the nucleus size.

In this Article, we introduce a computational method that addresses the limitations of the seeding technique. Like seeding, it relies on classical nucleation theory to estimate the nucleation barrier. However, it borrows ideas from Umbrella Sampling to improve this estimate. This combination results in Variational Umbrella Seeding, a method for estimating the barrier that is faster than Umbrella Sampling, while being more accurate than seeding.

I. SEEDING AND UMBRELLA SAMPLING

Before explaining our new method, we will first review two well-established popular methods for calculating nucleation barriers: Seeding¹⁰ and Umbrella Sampling.⁶ In Figure 1, we show schematic representations of Seeding and Umbrella Sampling.

In the seeding approach, the initial configuration consists of a nucleus - the 'seed' - which is embedded within the metastable parent phase. Subsequently, simulations are performed to determine whether this seed grows or shrinks. By

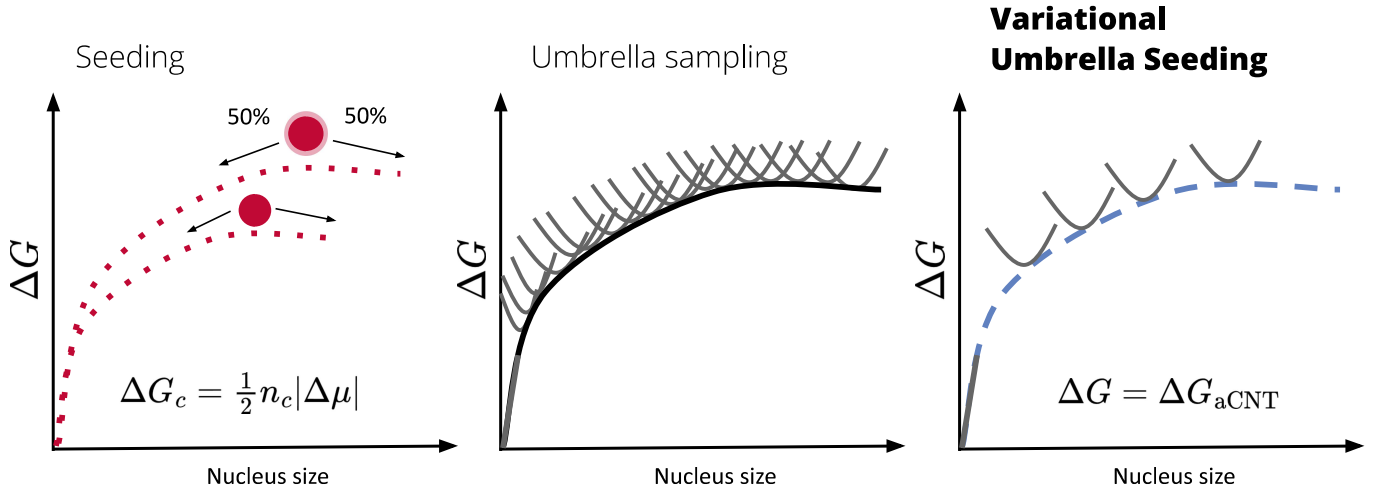


FIG. 1. Schematic comparison of Seeding, Umbrella Sampling, and Variational Umbrella Seeding, illustrating how they estimate the nucleation barrier ΔG as a function of nucleus size. Seeding employs the CNT approximation, $\Delta G^c = n_c |\Delta \mu|/2$, based on the number of particles in the critical nucleus size, n_c , for estimating the barrier height. This makes Seeding dependent on the choice of order parameter for computing the nucleus size. In contrast, Umbrella Sampling and Variational Umbrella Seeding are independent of the choice of order parameter. Umbrella Sampling does not rely on CNT and uses a large number of biased simulations (grey parabolas) to construct the nucleation barrier. Variational Umbrella Seeding relies on an adjusted version of CNT (aCNT) and uses a small number of biased simulations to construct the barrier.

varying the temperature or the pressure, seeding identifies the conditions under which the seed grows and shrinks with equal probability. This seed defines the critical nucleus under these conditions. Using the CNT approximation, Equation (2), we can calculate the height of the nucleation barrier $\Delta G_{\text{CNT}}^c = n_c |\Delta \mu|/2$. This approximation has been shown to give accurate results for condensation, freezing, and melting of various systems such as Lennard-Jones, hard spheres, water, and NaCl.^{10–18} Moreover, by relying on CNT, seeding requires only one piece of information from simulation: the critical nucleus size. This fact makes it very efficient and is the main advantage of seeding.

However, the CNT approximation, Equation (2), depends on the criterion chosen to measure the nucleus size. In Figure 1, the two red dots represent the *same* critical nucleus measured with two different criteria. A looser criterion will classify more particles as part of the nucleus. This is visualized by the light red layer of particles on the surface of the nucleus. Consequently, employing a looser criterion, results in a larger critical nucleus size, and therefore a higher barrier height. In summary, using two different criteria will yield estimates of different critical nucleus sizes, and as a result different barrier heights.

In contrast, Umbrella Sampling does not rely on CNT and depends only marginally on the chosen criterion for measuring the nucleus size.¹⁹ Umbrella Sampling uses a large number of biased simulations to measure the free-energy profile. Typically, parabolic bias potentials, depicted as grey overlapping parabolas in Figure 1, are used. Each parabola represents a separate biased simulation, where the bias potential serves to constrain the nucleus size. Essentially, by measuring the gradient along the entire free-energy profile, Umbrella Sampling effectively integrates the nucleation barrier in incremental steps. Although Umbrella Sampling does not rely on CNT,

the requirement to use a substantial number of biased simulations makes Umbrella Sampling considerably slower than seeding.

The idea of Variational Umbrella Seeding is to combine the strengths of Seeding as well as of Umbrella Sampling. By using an adjusted classical nucleation theory (aCNT), this approach eliminates the dependence of Seeding on the criterion chosen for measuring the nucleus size. At the same time, using aCNT also significantly reduces the number of biased simulations that are required to compute the barrier. In Figure 1, we illustrate this by drawing only four parabolas instead of the many needed for Umbrella Sampling.

II. ADJUSTED CLASSICAL NUCLEATION THEORY

Before introducing the adjusted classical nucleation theory (aCNT), we take a step back to the origin of the CNT expression, Equation (2). For the purpose of generality, we consider a generic scenario where a nucleus of a ‘child’ phase forms from a ‘parent’ phase in the grand canonical (μVT) ensemble. According to CNT, the nucleation barrier is determined by two competing factors: the volume v of the nucleus and the interface separating the nucleus from the parent phase. Without assuming a specific shape of the nucleus, we can write the area of this interface as $\alpha v^{2/3}$, where α is a dimensionless proportionality constant. Since $v^{1/3}$ is proportional to the linear dimension of the nucleus, it follows that the interfacial area is proportional to the square of the linear dimension.²⁰ The grand potential of a nucleus with volume v is then given by

$$\Delta \Omega_{\text{CNT}}(v) = \alpha v^{2/3} \gamma - v |\Delta p|, \quad (3)$$

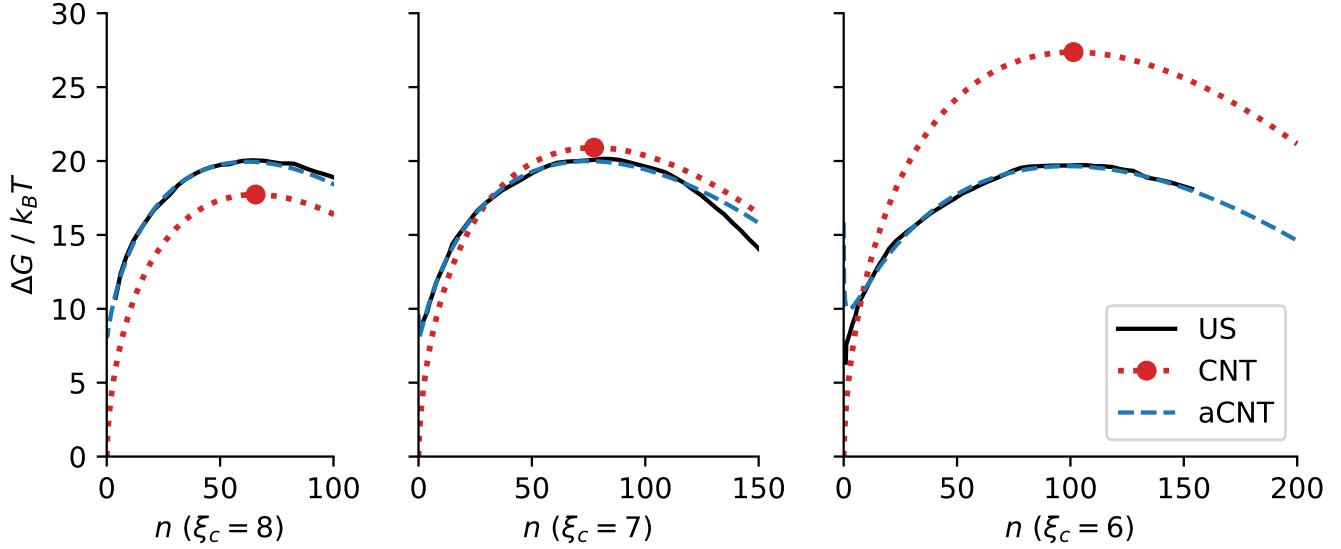


FIG. 2. The Gibbs free energy $\Delta G(n)/k_B T$ for the formation of a crystal nucleus of size n from a fluid of hard spheres at a pressure of $P\sigma^3/k_B T = 17.0$. The black lines represent Umbrella Sampling results from Ref. 19. The blue lines denote aCNT fits of the nucleation barriers, while the red dots and red dotted lines are CNT approximations of the barrier.

where γ is the interfacial tension and Δp is the Laplace pressure, i.e. the pressure difference between the child and parent phase at equal chemical potential. Maximizing $\Delta\Omega_{\text{CNT}}(v)$ with respect to v yields the critical nucleus size v_c , which is related to the interfacial tension γ as

$$2\alpha\gamma = 3v_c^{1/3}|\Delta p|. \quad (4)$$

For a spherical nucleus of radius r , this becomes the familiar Laplace equation, $|\Delta p| = 2\gamma/r$. Substituting Equation (4) into Equation (3) yields the barrier height

$$\Delta\Omega_{\text{CNT}}^c = \frac{4(\alpha\gamma)^3}{27|\Delta p|^2} = \frac{1}{2}v_c|\Delta p|. \quad (5)$$

Now, the underlying approximations of Equation (5) become clearer. Essentially, the interfacial tension is determined by the critical nucleus size via Equation (4). This implies that the Laplace equation is implicitly contained in Equation (5). Therefore, using Equation (5), we assume that the criterion chosen for measuring the size of the nucleus corresponds to the interface of tension.¹¹ If this assumption does not hold, Equation (4) will give an incorrect value for the interfacial tension and therefore an inaccurate value for the height of the barrier.

In simulations of nucleation, it is more common to measure the Gibbs free-energy barrier ΔG in the isobaric-isothermal (NPT) ensemble. As Ref. 23 discusses, the free-energy difference with respect to the homogeneous parent phase remains the same, i.e. $\Delta\Omega = \Delta G$. Therefore, the Gibbs free-energy barrier is given by

$$\Delta G_{\text{CNT}}(v) = \alpha v^{2/3}\gamma - v|\Delta p|, \quad (6a)$$

$$2\alpha\gamma = 3v_c^{1/3}|\Delta p|, \quad (6b)$$

$$\Delta G_{\text{CNT}}^c = \frac{4(\alpha\gamma)^3}{27|\Delta p|^2} = \frac{1}{2}v_c|\Delta p|. \quad (6c)$$

From now on, we always assume an isobaric-isothermal (NPT) ensemble, so we focus on the Gibbs free-energy barrier ΔG for nucleation.

In the context of crystal nucleation, the Gibbs free-energy barrier $\Delta G(n)$ is usually measured as a function of the number of particles n in the nucleus at a fixed pressure. The CNT equations corresponding to Equations (6a) to (6c) become as follows²⁰

$$\Delta G_{\text{CNT}}(n) = \alpha n^{2/3}\gamma - n|\Delta\mu|, \quad (7a)$$

$$2\alpha\gamma = 3n_c^{1/3}|\Delta\mu|, \quad (7b)$$

$$\Delta G_{\text{CNT}}^c = \frac{4(\alpha\gamma)^3}{27|\Delta\mu|^2} = \frac{1}{2}n_c|\Delta\mu|. \quad (7c)$$

In these equations, $|\Delta\mu|$ is the difference in chemical potential between the solid and liquid phase at equal pressure, and n_c denotes the number of particles in the critical nucleus. The proportionality constant α is now expressed in units of area. Again, it is important to note that the criterion used to measure the nucleus size n will influence the value of the interfacial tension γ and therefore the height of the barrier.

To illustrate this issue, we show in Figure 2 Umbrella Sampling simulations of hard-sphere nucleation as described in Ref. 19. These crystal nucleation barriers were measured at a pressure $P\sigma^3/k_B T = 17$, corresponding to a metastable fluid packing fraction of $\eta = 0.5352$, a supersaturation of $|\Delta\mu| = 0.54 k_B T$, and a barrier height $\Delta G^c = 19.7 \pm 0.3 k_B T$.

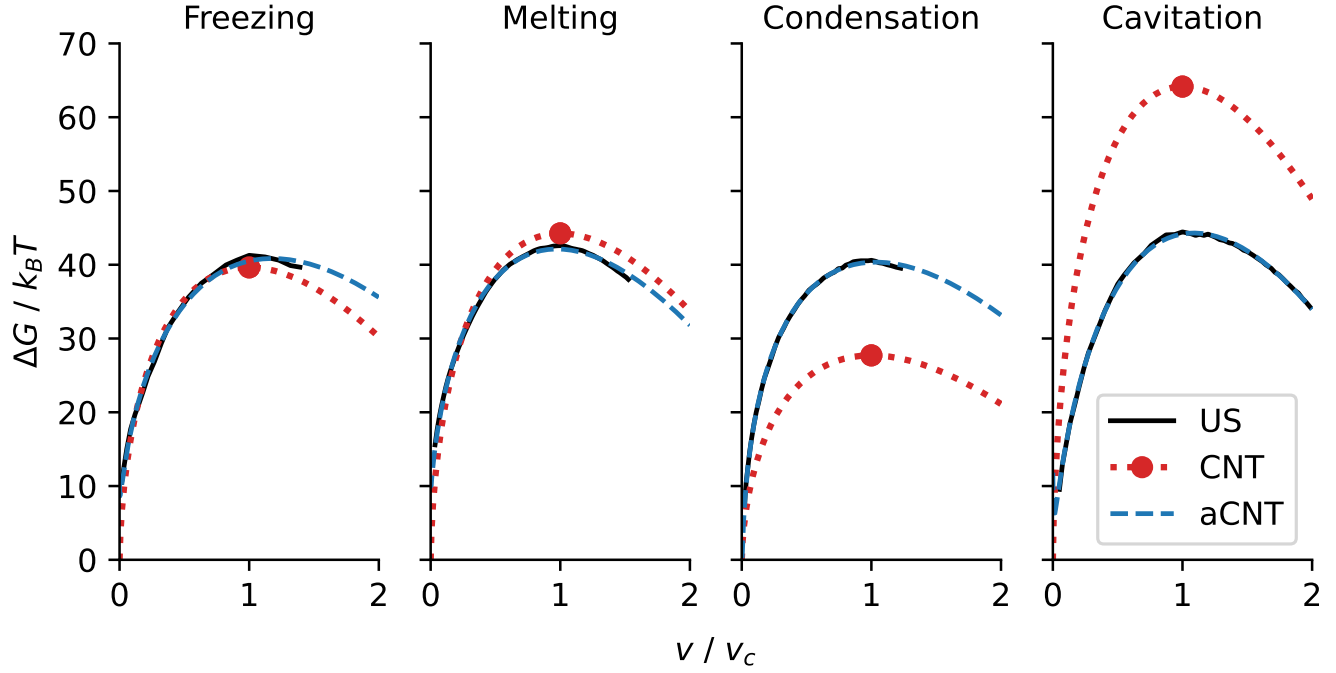


FIG. 3. The Gibbs free energy $\Delta G(v)/k_B T$ for nucleation during freezing¹⁹ and melting¹⁸ of hard spheres, condensation of Lennard-Jones,²¹ and cavitation of water.²² The size of the nucleus v is normalized by the critical nucleus size v_c . The solid black lines are the Umbrella Sampling measurements of Refs. 18,19,21,22. The dashed blue lines denote aCNT fits of the nucleation barriers, while the red dots and red dotted lines are CNT approximations of the barrier.

We show three different barriers, each measured with a different criterion to distinguish the crystal nucleus from the surrounding fluid. To be precise, the number of solid-like bonds ξ_c used to classify a particle as solid-like was varied. Remarkably, the barrier height ΔG^c measured via Umbrella Sampling is almost independent of the criterion. In contrast, the critical nucleus size n_c varies significantly. For $\xi_c = 8$, the critical nucleus size is $n_c = 72$, while for $\xi_c = 6$, it is $n_c = 102$. Substituting these values into Equation (7c), we obtain nucleation barriers varying from $19 k_B T$ to $28 k_B T$. We have plotted these approximations as red dots in Figure 2. In this case $\xi_c = 7$ shows the best agreement with Umbrella Sampling. For $\xi_c = 8$, the barrier is underestimated due to a too stringent criterion, whereas for $\xi_c = 6$, the barrier is overestimated because the criterion is too loose.

Apart from examining the height of the barrier, we can also investigate the shape of the barrier. By leveraging the critical nucleus size n_c , we can estimate the interfacial tension γ using Equation (7b). In Figure 2, we plot the CNT nucleation barrier, Equation (7a), using this approximation for the interfacial tension as a red dotted line. We see that these representations deviate significantly from the Umbrella Sampling results denoted in black. Even in the best case of $\xi_c = 7$, we see that the CNT expression for the barrier fails to accurately capture the shape of the barrier. In short, this example of hard-sphere nucleation demonstrates that with an ill-defined nucleus size, the CNT equations do not capture the height and shape of the nucleation barrier.

In the literature, numerous efforts have been made to refine CNT to offer a more precise description of the shape of the nucleation barrier. For instance, Merikanto *et al.*²⁴ observed deviations in the initial part of the barrier for condensation. They proposed that this effect could be accounted for by a vertical shift of the free-energy barrier, essentially an additive term in Equation (7a). Additionally, Prestipino, Laio, and Tosatti²⁵ introduced corrections to accommodate a non-sharp and thermally fluctuating interface. Firstly, they added a logarithmic term proportional to $\log(r)$, where r denotes the radius of the nucleus. Secondly, they replaced the constant interfacial tension γ with a function $\gamma(r) = \gamma_0(1 - 2\delta/r + \epsilon/r^2)$, in essence representing curvature corrections to the interfacial tension. They noted that the logarithmic correction has a considerably smaller effect on the quality of the fit than the curvature corrections to the interfacial tension. Finally, Filion *et al.*¹⁹ suggested that the effect of different order parameters can be captured by a shift in the radius. They proposed to replace the measured radius r by $r - \delta$ in the CNT equations.

Rather than selecting one of these modifications, we propose the following expressions for the shape of the nucleation barrier

$$\Delta G_{\text{aCNT}}(v) = -v|\Delta p| + g'_2 v^{2/3} + g'_1 v^{1/3} + g'_0, \quad (8a)$$

$$\Delta G_{\text{aCNT}}(n) = -n|\Delta \mu| + g_2 n^{2/3} + g_1 n^{1/3} + g_0. \quad (8b)$$

In these expressions, g'_i and g_i are fitting parameters for the nucleation barrier. Following Ref. 19, we refer to Equations (8a) and (8b) as the adjusted classical nucleation theory (aCNT)

expressions for the nucleation barrier. In contrast to Refs. 19,24,25, we do not assign a specific physical interpretation to these parameters. However, we note that all their corrections, except for the logarithmic term, are captured by these aCNT expressions.

To validate the aCNT expressions, we use Equation (8b) to fit the Umbrella Sampling barriers of hard-sphere crystal nucleation. We show these fits as dashed blue lines in Figure 2. During the fitting procedure, we kept the supersaturation $|\Delta\mu| = 0.54 k_B T$ fixed, as determined by thermodynamic integration of the equation of state. The remaining three parameters g_0, g_1, g_2 are fitted to the Umbrella Sampling data. More specifically, they were fitted to the part of the nucleation barrier where the nucleus size n obeys $5 < n < n_c$. In this regime, the barrier as measured by Umbrella Sampling deviates less than $0.4 k_B T$ from the aCNT fit. From this comparison, it is evident that the aCNT expression effectively captures the shape of the nucleation barrier of hard spheres, as measured with different order parameters.

As a further illustration, we investigate four different nucleation barriers previously measured using Umbrella Sampling for various phase transitions: crystal nucleation,¹⁹ crystal melting,¹⁸ cavitation,²² and condensation.²¹ In Figure 3, the measured barriers are denoted as solid black lines. The CNT approximations of these barriers, Equations (6a) to (6c), based on the volume v_c of the critical nucleus are represented as red dots and red dotted lines. We observe that the freezing and melting barriers are reasonably well described by the CNT approximation. However, the condensation barrier is severely underestimated by CNT, while the cavitation barrier is severely overestimated. It is important to stress again that the accuracy of the CNT approximation depends critically on the criterion used to identify the nucleus. For instance, for condensation and cavitation, the ‘equidensity’ criterion has been shown to be a reasonable choice.²¹ Next, we employ the aCNT expression, Equation (8a), to fit the barriers. In this case, the Laplace pressure $|\Delta p|$ is determined by thermodynamic integration of the equation of state, while the remaining three parameters g'_0, g'_1, g'_2 are fitted to the Umbrella Sampling data. The resulting fits are shown with dashed blue lines. It is evident that the shape of all these nucleation barriers can be well described with aCNT.

III. METHOD

The effectiveness of aCNT in describing the nucleation barrier of crystallization, cavitation, condensation, and melting, suggests a strategy for approximating the nucleation barrier height: By fitting the parameters g_0, g_1, g_2 in Equation (8), the height of the barrier can be determined without the need of performing full Umbrella Sampling calculations. In this Section, we will introduce Variational Umbrella Seeding as an efficient implementation of this idea.

Variational Umbrella Seeding combines ideas from both Seeding and Umbrella Sampling. In Figure 4, we provide a schematic overview of the method. It employs Seeding to offer a first estimate of the critical nucleus size and to provide

initial configurations. Starting from these initial configurations, we use Umbrella Sampling to measure segments of the nucleation barrier. Subsequently, these barrier segments are fitted to an aCNT expression to approximate the full nucleation barrier.

A. Seeding: critical nucleus and initial configurations

The first step in Variational Umbrella Seeding is to determine the critical nucleus size and to generate some initial configurations. The Seeding technique is very efficient for this purpose. The result of the seeding technique is a configuration of a nucleus under the conditions for which this nucleus is critical. Hence, we already possess a good estimate of the critical nucleus size n_c . By starting simulations from the critical nucleus, we can select those simulations for which the nucleus shrinks. From these trajectories, we can then readily select initial configurations of nucleus sizes ranging from 0 to n_c .

B. Measure barrier segments with Umbrella Sampling

The second step involves measuring segments of the nucleation barrier using Umbrella Sampling. As illustrated in Figure 4, only four of these barrier fragments are required.

To perform these simulations, we employ the hybrid Monte Carlo method as a popular way for performing Umbrella Sampling simulations of nucleation barriers.^{26–28} The main advantage of hybrid Monte Carlo over traditional Monte Carlo is that it allows the use of highly optimized and parallelized molecular dynamics codes such as LAMMPS²⁹ and GROMACS.³⁰

In essence, hybrid Monte Carlo combines Monte Carlo simulation with molecular dynamics (MD) simulations to propose trial moves for Monte Carlo (MC). Each MC cycle consists of the following steps. First, initial velocities are generated for each particle according to a Maxwell-Boltzmann distribution. Subsequently, a short trajectory is simulated using MD. The trajectory is accepted or rejected according to a Metropolis criterion based on the total energy of the system.

We constrain the nucleus size by adding an external bias potential to the total energy in the Metropolis acceptance step. To elaborate, after each MD trajectory, we accept the trajectory with a probability p_{acc} given by

$$p_{\text{acc}} = \min(1, \exp(-\Delta H/k_B T)), \quad (9)$$

$$H = K + U_{\text{pot}} + U_{\text{ext}}(n), \quad (10)$$

$$U_{\text{ext}}(n) = \frac{1}{2}k(n - \hat{n})^2. \quad (11)$$

In these equations, ΔH represents the change in the total energy H of the system, which consists of the kinetic energy $K = \sum_i \mathbf{p}_i^2/2m_i$, potential energy $U_{\text{pot}} = \sum_{i<j} \phi(r_{ij})$ and the external bias potential U_{ext} with \mathbf{p}_i and m_i the momentum and mass of particle i , respectively, and $\phi(r_{ij})$ the pair interaction between particle i and j . The external bias potential U_{ext} is

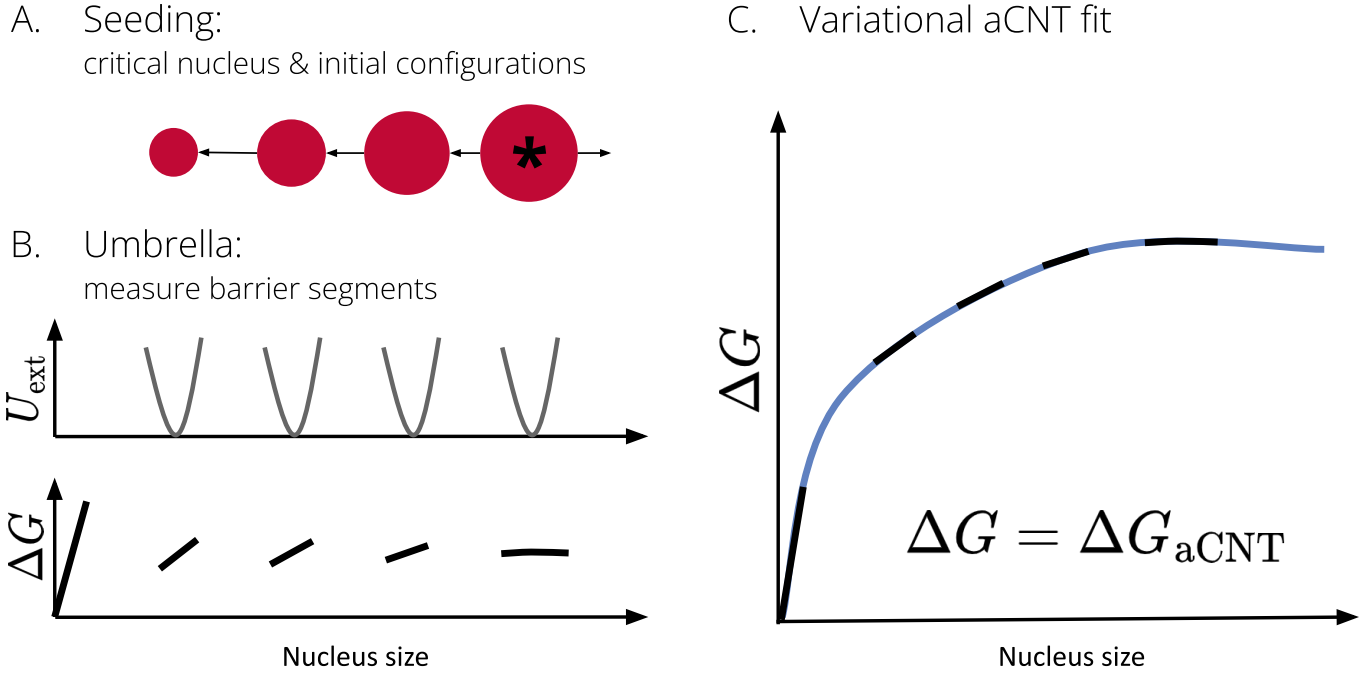


FIG. 4. Schematic overview of Variational Umbrella Seeding. A. Initially, Seeding is employed to estimate the critical nucleus size and to prepare initial configurations. B. Subsequently, Umbrella Sampling is used to measure segments of the nucleation barrier. C. Finally, an adjusted version of CNT (aCNT) is employed to construct the entire nucleation barrier from these barrier fragments.

employed to keep the nucleus size n close to the target size \hat{n} . The spring constant k determines the stiffness of the bias potential. The result of such a simulation is a biased time series of nucleus sizes $n(t)$. This time series is subsequently converted into a biased nucleus size distribution $p(n)$. From this biased nucleus size distribution, we can estimate the unbiased free-energy profile

$$G(n)/k_B T = -\ln p(n) - U_{\text{ext}}(n)/k_B T + \text{constant}. \quad (12)$$

To sample the isobaric-isothermal (NPT) ensemble, we consider two approaches. The first approach is to use an NVE integrator for the MD trajectories and perform volume moves after each trajectory. Trajectories are accepted according to Equation (9) and the volume moves according to standard volume move acceptance criteria, taking the bias potential into account. By using a symplectic and time-reversible NVE integrator, this scheme guarantees that detailed balance is obeyed.³¹

Alternatively, Gonzalez *et al.*²⁶ showed that an NPT integrator can also be employed for the MD trajectories. In this case, no separate volume moves are performed. Trajectories are accepted with a probability

$$p_{\text{acc}} = \min(1, \exp(-\Delta U_{\text{ext}}/k_B T)). \quad (13)$$

Although this scheme does not guarantee detailed balance, Gonzalez *et al.*²⁶ showed that this approach provides an excellent approximation provided that the MD time step is small enough and the MD trajectories are long enough.

To evaluate our hybrid Monte Carlo methods, we measured the density and potential energy of the homogeneous liquid

phase without an external bias, i.e. $U_{\text{ext}} = 0$ in both Equation (9) and Equation (13). In this way, we can compare the density and potential energy directly to a standard unbiased MD simulation, where velocities are not resampled. In all cases, we made sure that the relative error in both the density and potential energy was less than 0.05%.

Variational Umbrella Seeding relies on a small number of biased simulations. Similarly to Umbrella Sampling, these simulations should be evenly distributed across the nucleation barrier. We found that employing four different simulations, with target sizes $\hat{n} = n_c/4, n_c/2, 3n_c/4$, and n_c , yields reliable results. This means that having a rough estimate of the critical nucleus size n_c before starting the simulations, is useful but this estimate does not need to be accurate. This estimate of the critical nucleus size aids in selecting the spring constant k of the bias potential. In Appendix D, we describe our approach for optimizing these parameters of Variational Umbrella Seeding using tests with an idealized nucleation barrier.

C. Variational aCNT fit of the nucleation barrier

A nucleation barrier is usually constructed from a sequence of biased simulations by ‘stitching’ together many overlapping free-energy profiles. Common approaches for this task include the Multistate Bennett Acceptance Ratio (MBAR) method or the Weighted Histogram Analysis Method (WHAM). In order to take advantage of the aCNT, Equation (8), we adopt a different approach to process the simulation data. We employ a maximum-likelihood approach to fit the parameters g_1 and g_2 , and use a separate unbiased

simulation to fit g_0 .

To illustrate the maximum-likelihood approach, we first compute the likelihood of a series of measurements, under the assumption that the aCNT Equation (8) holds for certain values of the parameters g_i . In this case, the nucleation barrier and the external bias potential U_{ext} generate a probability distribution $p(n)$ for the nucleus size, given by

$$p(n) = \frac{1}{Z} \exp[-(\Delta G_{\text{aCNT}}(n) + U_{\text{ext}}(n))/k_B T], \quad (14)$$

$$Z = \sum_n \exp[-(\Delta G_{\text{aCNT}}(n) + U_{\text{ext}}(n))/k_B T]. \quad (15)$$

We note that the normalization factor Z depends on both the aCNT parameters g_i and the bias potential U_{ext} , but Z can easily be computed. The likelihood L of a series of independent measurements $n(t)$ is given by

$$L(n(t)) = \prod_t \frac{1}{Z} \exp[-(\Delta G_{\text{aCNT}}(n(t)) + U_{\text{ext}}(n(t)))/k_B T] \quad (16)$$

where t is the simulation time. With a logarithmic transformation, this becomes the log-likelihood ℓ given by

$$\ell(n(t)) = -\sum_t [\ln Z + (\Delta G_{\text{aCNT}}(n(t)) + U_{\text{ext}}(n(t)))/k_B T]. \quad (17)$$

Finally, the total log-likelihood of multiple simulations is the sum of the individual log-likelihood functions

$$\ell(n_1(t), \dots) = \sum_i \ell_i(n_i(t)). \quad (18)$$

Here ℓ_i represents the likelihood of the series of measurements $n_i(t)$ in simulation i . One subtlety in this derivation is that we assumed that the measurements $n(t)$ are independent of each other. However, the measurements $n(t)$ originate from a correlated time series, thus this assumption does not automatically hold. To solve this issue, we estimate the autocorrelation time τ of the time series $n(t)$ as the time at which its normalized autocorrelation function has decayed to $1/e$. We employ subsampling to obtain independent samples: rather than using the entire series $n(t)$ to compute the log-likelihood Equation (17), we only use a subset t_1, t_2, \dots with a separation equal to the autocorrelation time i.e. $t_{i+1} = t_i + \tau$.

In short, for a given set of aCNT parameters g_i , we use Equation (18) to compute the log-likelihood of our observations $n_i(t)$. The maximum likelihood estimator for g_1, g_2 is consequently the set of parameters \hat{g}_1, \hat{g}_2 that maximizes the log-likelihood. We note that this maximum-likelihood approach is very similar to the Variational Free-Energy Profile (VFEP)³² method, which was proposed in the context of biomolecular reactions. However, instead of using a generic spline interpolation function, we take advantage of the aCNT Equation (8) to improve the efficiency of the method.

Because g_0 is an additive term in the nucleation barrier, the log-likelihood Equation (18) is independent of g_0 . To fit g_0 , we perform an independent and unbiased simulation of the metastable liquid. In this way, we also measure the full nucleus size distribution $p(n)$ of the metastable liquid, and we

do not rely on aCNT to determine the shape of this initial part of the nucleation barrier. The initial part of the nucleation barrier is then given by

$$\Delta G(n) = -\ln \left(\frac{p(n)}{N} \right). \quad (19)$$

To be precise, when we refer to $p(n)$, we denote the average number of nuclei of size n in a system of N particles. In this way, Equation (19) quantifies the free energy with the homogeneous liquid serving as the reference state.³³ Subsequently, the unbiased initial part of the barrier ΔG is ‘glued’ to the aCNT barrier, and this ‘glueing’ process determines the value of g_0 . To establish this, we determine the nucleus size n_0 for which $\Delta G(n_0) \approx 10 k_B T$. Subsequently, we determine g_0 such that the equality

$$\Delta G_{\text{aCNT}}(n_0|g_i) = \Delta G(n_0) \quad (20)$$

is satisfied.

Finally, when we have fitted the aCNT parameters g_i , we obtain the Variational Umbrella Seeding estimate for the nucleation barrier height simply as the maximum of the aCNT Equation (8).

D. Pressure/temperature dependence of the nucleation barrier

Up to this point, we have described the procedure for employing Variational Umbrella Seeding to obtain an estimate of the nucleation barrier ΔG^c for a single state point. Once the nucleation barrier is estimated for several state points, we can fit them with a CNT expression to obtain the pressure or temperature dependence of the nucleation barrier. This process closely resembles that of the Seeding approach, with one notable exception: the approximation of the interfacial tension. From a Variational Umbrella Seeding estimate ΔG_{aCNT}^c , we compute the interfacial tension using Equation (7c) as follows

$$\alpha\gamma = \left(\frac{27\Delta G_{\text{aCNT}}^c |\Delta\mu|^2}{4} \right)^{1/3}. \quad (21)$$

In the Seeding approach, the interfacial tension is directly determined by the critical nucleus size n_c . In contrast, here we determine the interfacial tension from the barrier height ΔG_{aCNT}^c . For a spherical nucleus, this can be expressed as

$$\gamma = \left(\frac{3\Delta G_{\text{aCNT}}^c |\Delta\mu|^2 \rho_s^2}{16\pi} \right)^{1/3}, \quad (22)$$

where ρ_s is the density of the solid phase. Subsequently, similar to the Seeding approach, the interfacial tension $\gamma(p, T)$ is fitted as a function of pressure or temperature. The fit is usually linear¹⁰, but if the data suggests otherwise, one can fit to another functionality. The pressure and temperature depen-

dence of the nucleation barrier is then given by

$$\Delta G_{\text{aCNT}}^c(p, T) = \frac{4(\alpha\gamma(p, T))^3}{27|\Delta\mu(p, T)|^2}, \quad (23a)$$

$$\Delta G_{\text{aCNT}}^c(p, T) = \frac{16\pi(\gamma(p, T))^3}{3|\Delta\mu(p, T)|^2\rho_s(p, T)^2}. \quad (23b)$$

Again, the second equation refers to the case of a spherical nucleus. We emphasize that both Equations (23a) and (23b) yield identical results for $\Delta G_{\text{aCNT}}^c(p, T)$, irrespective of the actual shape of the nucleus. Imposing a specific nucleus shape is only necessary for the interpretation of the interfacial tension. To calculate the nucleation rate, we also require the kinetic prefactor. This is exactly the same as in Seeding¹⁰ and in Umbrella Sampling.^{6,33}

IV. RESULTS AND DISCUSSION

We assess the performance of Variational Umbrella Seeding on crystal nucleation in three distinct systems: nearly hard spheres (WCA), monatomic water (mW), and the TIP4P/ICE model of water.

A. Nearly hard spheres (WCA)

We simulate hard spheres using a Weeks-Chandler-Andersen (WCA) potential. This potential is the repulsive part of the Lennard-Jones pair potential and is widely used in molecular dynamics simulations to model hard spheres. In Ref. 34, it was demonstrated that an effective hard-sphere diameter $\sigma_{\text{eff}} = 1.097\sigma$ effectively captures the free energy and nucleation rates of hard spheres. This effective hard-sphere diameter is defined such that the freezing density of the WCA system maps onto the freezing density of the hard-sphere system. Following Ref. 34, we measure the nucleation barrier at a temperature of $k_B T/\epsilon = 0.025$ and a pressure of $P\sigma^3/k_B T = 12.0$. We simulate $N = 2 \times 10^4$ particles, employing a time step of $0.001\tau_{\text{MD}}$, where $\tau_{\text{MD}} = \sqrt{m\sigma^2/k_B T}$ represents the molecular dynamics unit of time. The temperature and pressure are maintained fixed with a Nosé-Hoover thermostat and barostat with relaxation times of $0.1\tau_{\text{MD}}$ and $0.5\tau_{\text{MD}}$, respectively. To measure the nucleus size, we use the same order parameter as in Ref. 34. To be precise, we calculate a spherical harmonics expansion q_{lm} of the nearest neighbor density, where we use a cutoff of 1.5σ to identify nearest neighbors. Next, we compute inner products $q_l(i, j)$ between the q_{lm} vectors of neighboring particles, and identify a solid-like bond as a pair of particles (i, j) for which $q_l(i, j) > 0.7$. A particle is solid-like if it has ξ_c or more solid-like bonds. We explore different values of $\xi_c = 6, 7, 8$ to investigate the effect of different order parameters. Finally, the largest cluster of solid-like particles is identified as the crystal nucleus. Based on Ref. 34, we use the following initial estimates for the critical nucleus sizes: $n_c = 185, 155$, and 130 for $\xi_c = 6, 7, 8$, respectively. As described in Section III B, these estimates

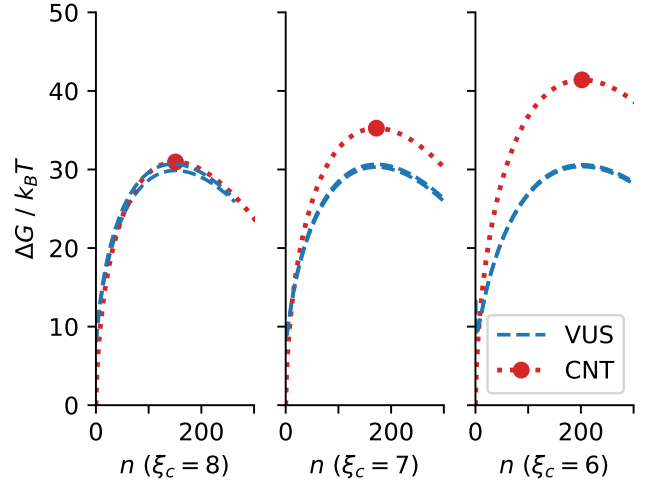


FIG. 5. The free-energy barrier $\Delta G(n)/k_B T$ for the formation of a crystal nucleus of size n from a fluid of nearly hard spheres (WCA) at a pressure $P\sigma^3/k_B T = 12.0$ and temperature $k_B T/\epsilon = 0.025$, for different order parameter thresholds ξ_c . A particle is classified as solid-like if it has at least ξ_c solid-like bonds, with $\xi_c = 6, 7, 8$. The red dots and red dotted lines represent CNT approximations, Equation (7a), of the barrier based on the critical nucleus size n_c . The blue dashed lines are aCNT approximations of the barrier derived from Variational Umbrella Seeding (VUS) simulations. Note that two aCNT approximations are shown for each order parameter threshold ξ_c : one for the approximate NPT and one for the rigorous NVE integrator used in the hybrid Monte Carlo simulations. As they are almost indistinguishable, we do not label them separately.

also determine the target sizes and spring constants in the hybrid Monte Carlo simulations. In these simulations we use short molecular dynamics trajectories with a length of $0.5\tau_{\text{MD}}$ amounting to a total simulation time of $100,000\tau_{\text{MD}}$ for each target size. We used the first $10,000\tau_{\text{MD}}$ for equilibration and the following $90,000\tau_{\text{MD}}$ for production. We found the auto-correlation time to be approximately $100\tau_{\text{MD}}$.

With our results for nearly hard spheres, we can illustrate the order-parameter independence of Variational Umbrella Seeding. The nucleation barrier height is nearly independent of the order parameter threshold ξ_c that is used to identify the crystal nucleus: while varying ξ_c from 6 to 8, the nucleation barriers estimated by Variational Umbrella Seeding varies less than $1 k_B T$. In contrast, the critical nucleus size n_c depends sensitively on the chosen order parameter. Consequently, the CNT approximation $\Delta G^c = n_c |\Delta\mu|/2$ also relies heavily on the order parameter. For nearly hard spheres, the CNT approximation decreases from $\Delta G^c = 40.8 k_B T$ to $\Delta G^c = 30.8 k_B T$ when changing the order parameter from $\xi_c = 6$ to $\xi_c = 8$. In Figure 5, we illustrate the order-parameter independence of Variational Umbrella Seeding. The red dotted lines represent CNT approximations of the nucleation barrier based on the critical nucleus size, whereas the dashed blue lines are the aCNT fits from the Variational Umbrella Seeding simulations. For $\xi_c = 8$, these barriers are nearly identical. However, for $\xi_c = 7$ and $\xi_c = 6$, the critical nucleus size increases,

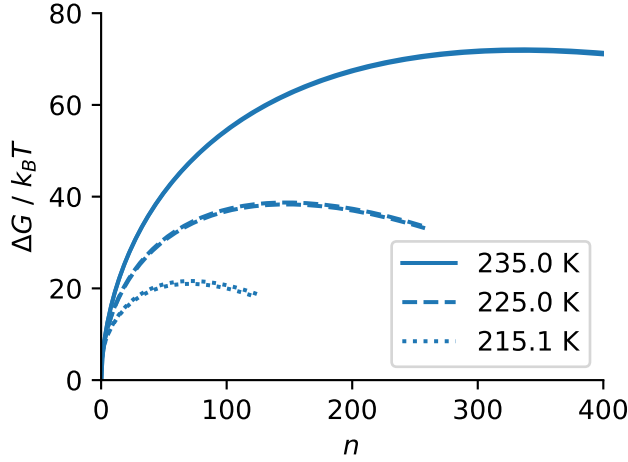


FIG. 6. Free-energy barriers $\Delta G(n)/k_B T$ for the formation of a crystal nucleus of size n from an mW liquid at zero pressure for different temperatures T . The blue lines are aCNT approximations of the barrier based on Variational Umbrella Seeding (VUS) simulations. Note that two aCNT approximations are shown for each temperature: one for the approximate NPT and one for the rigorous NVE integrator for the hybrid Monte Carlo simulations. As they are almost indistinguishable, we do not label them separately.

and the CNT approximation overestimates the barrier height. Additionally, we observe that the approximate NPT and the rigorous NVE integrator yield almost identical results for the nucleation barrier. In Figure 5, we plotted the nucleation barriers from both schemes, i.e. one blue dashed line corresponds to the NPT and one to the NVE integrator. Since these lines almost exactly overlap, we conclude that these schemes give almost identical results.

B. Monatomic water (mW)

The second model we investigate is the monatomic model of water (mW).³⁶ Following Ref. 35, we study three different temperatures: $T = 215.1$ K, 225.0 K, and 235.0 K, while fixing zero pressure. The melting temperature for this model at zero pressure is $T_m = 274.6$ K.³⁶ For 215.1 K and 225.0 K, we use $N = 2000$ particles, and for 235.0 K, we employ $N = 4000$ particles, following Ref. 37. The timestep is 2 fs, and the temperature and pressure are fixed using a Nosé-Hoover thermostat and barostat with a relaxation time of 0.1 ps and 0.2 ps, respectively. Following Ref. 10, we identify the crystal nucleus as follows: we first compute the averaged bond-order parameter \bar{q}_6 . Employing a nearest-neighbor cutoff of 3.51 Å, solid-like particles are identified as $\bar{q}_6 > \bar{q}_6^c$, where the threshold \bar{q}_6^c depends on temperature as $\bar{q}_6^c = 0.5055 - 5.324 \times 10^{-4} T/\text{K}$. Based on the seeding simulations of Ref. 10, we use the following initial estimates for the critical nucleus sizes: $n_c = 70$, 150 , and 320 for $T = 215.1$, 225.0 , and 235.0 K, respectively. In our hybrid Monte Carlo scheme, we used short molecular dynamics trajectories with a length of 0.5 ps amounting to a

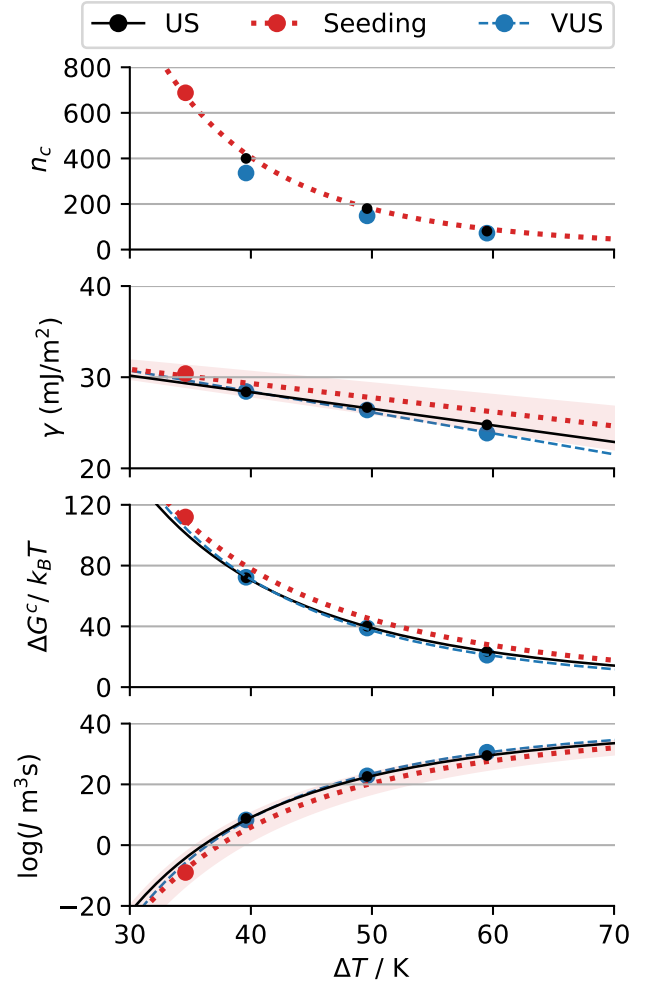


FIG. 7. Critical nucleus size n_c , interfacial tension γ , nucleation barrier $\Delta G^c/k_B T$, and decimal logarithm of the nucleation rate $J/\text{m}^3 \text{s}$ as a function of supercooling ΔT at zero pressure for the mW model of water. The black dots and solid lines are Umbrella Sampling (US) results from Ref. 35, the red dots and red dotted lines are Seeding results from Ref. 10, and the blue dots and dashed lines are our Variational Umbrella Seeding (VUS) results.

simulation time of 400 ns for each target size. We used the first 40 ns for equilibration and the following 360 ns for production. We determined an autocorrelation time of approximately 0.2 ns, which did not exhibit significant temperature dependence. To compute the nucleation rate from the nucleation barrier, we use a constant kinetic prefactor $J_0 = 5 \times 10^{39} \text{m}^{-3} \text{s}^{-1}$ because, within the temperature range we consider, it remains approximately constant. This kinetic prefactor is simply an average of the kinetic prefactors reported in Ref. 35.

In Figure 6, we plot our Variational Umbrella Seeding results for the nucleation barriers of mW. We present both the NPT and NVE integrator results simultaneously. Again, we observe that these schemes yield nearly identical results for the shape and height of the nucleation barrier.

In Figure 7, we show the critical nucleus size n_c , interfa-

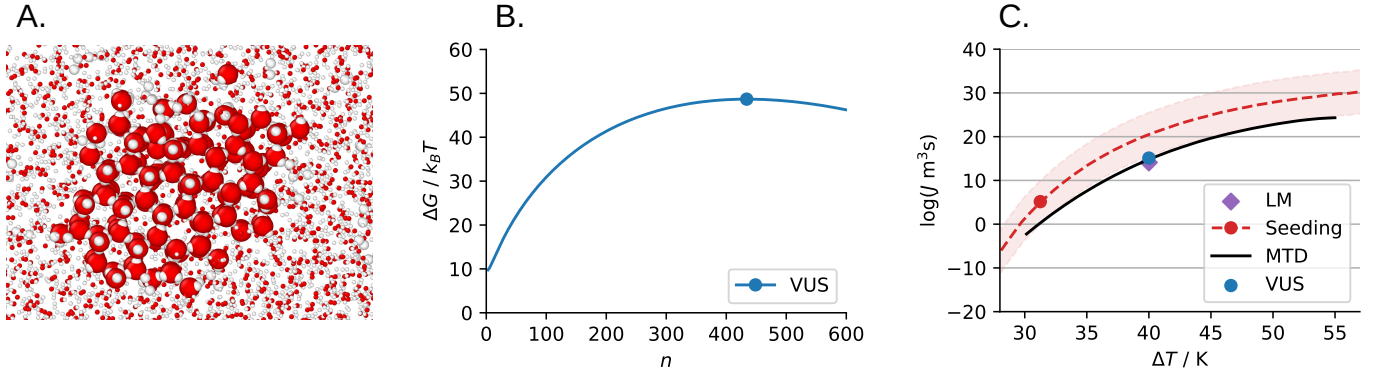


FIG. 8. Crystal nucleation of the TIP4P/ICE model of water at $p = 1$ bar. A. Cut-through image of a crystal nucleus of size $n \approx 240$ at $T = 230$ K. The nucleus is identified as the largest cluster of particles that have an averaged bond-order parameter $\bar{q}_6 > 0.378$. The surrounding particles are reduced in size for clarity. B. Free-energy barrier $\Delta G(n)/k_B T$ for the formation of a crystal nucleus of size n at $T = 230$ K. The blue line is the aCNT approximation of the barrier based on our Variational Umbrella Seeding (VUS) simulations. The blue dot marks the top of the barrier. C. Decimal logarithm of the nucleation rate Jm^3s as a function of supercooling ΔT . The red dashed line and red shaded region are Seeding results from Ref. 38, while the black solid line is from Metadynamics (MTD) simulations from Ref. 39. The purple diamond is from Lattice Mold (LM) simulations of Ref. 40. The blue dot is the Variational Umbrella Seeding (VUS) result of this work.

cial tension γ , barrier height ΔG^c , and nucleation rate J as a function of supercooling $\Delta T = T_m - T$ for mW. We compare our Variational Umbrella Seeding (VUS) results with previous Umbrella Sampling (US) results by Russo, Romano, and Tanaka³⁵ and Seeding results by Espinosa *et al.*¹⁰ Strictly speaking, the Seeding simulations¹⁰ were performed at 1 bar, whereas the Umbrella Sampling simulations³⁵ and our Variational Umbrella Seeding simulations were performed at zero pressure. Since the slope of the melting curve of ice Ih is on the order of $-(100 - 200)$ bar/K,⁴¹ from 1 bar to 0 bar the melting temperature changes less than 0.01 K. In the following analysis, we ignore this very minor difference.

At a supercooling of $\Delta T = 40$ K, one can see that the critical nucleus size n^* reported in Ref. 35 (black dot) differs slightly from our value (blue dot). As discussed before, this is simply a result of using different criteria to estimate the nucleus size. Using the CNT approximation, these different critical nucleus sizes automatically lead to different nucleation barriers and nucleation rates. The red-shaded regions in Figure 7 show the associated uncertainty in the nucleation barriers and rates. Espinosa *et al.*¹⁰ estimate that in this case, the dependence of Seeding on the choice of order parameter leads to an uncertainty of about four orders of magnitude in the nucleation rate.

As observed in the case of nearly hard spheres, Variational Umbrella Seeding exhibits no such order-parameter dependence. In Figure 7, we plot the Variational Umbrella Seeding estimates of the nucleation barrier and nucleation rate with blue dots and dashed blue lines. Additionally, we plot the Umbrella Sampling results of Ref. 35 in this figure using black dots and solid lines. Comparing Umbrella Sampling, Seeding, and Variational Umbrella Seeding, we see that they all show good agreement. As previously found, the mislabeling criterion is a very reasonable choice of order parameter for Seeding simulations. Notably, our Variational Umbrella Seeding results are almost indistinguishable from Umbrella Sampling.

C. TIP4P/ICE

The final model we investigate is the TIP4P/ICE model of water at $T = 230$ K and $p = 1$ bar, for which the melting temperature is $T_m = 270$ K.³⁸ We simulate $N = 5881$ molecules using a timestep of 2 fs, while both the Nosé-Hoover thermostat and barostat have a relaxation time of 2 ps. Pair interactions are truncated at 9.0 Å. For long-range Coulombic interactions, we use the pppm/tip4p particle-particle particle-mesh (PPPM) solver in LAMMPS⁴² with a relative error in forces of 10^{-5} . Additionally, we employ the Shake algorithm⁴³ to constrain the O-H bond lengths and H-O-H angles. As the Shake algorithm is not reversible, the NVE integrator does not guarantee detailed balance. Hence, we solely performed simulations using the approximate NPT integrator. Again, we use the averaged bond-order parameter \bar{q}_6 as an order parameter, with a cutoff of 3.51 Å. Using a linear extrapolation of the thresholds in Ref. 38, we choose the threshold $\bar{q}_6^c = 0.378$. Based on the Seeding simulations of Ref. 38, we use $n_c = 240$ as an initial estimate for the critical nucleus size. We used short molecular dynamics trajectories with a length of 20 ps amounting to a simulation time of 650 ns for each target size. We used the first 200 ns for equilibration and the following 450 ns for production. We found an autocorrelation time of approximately 20 ns.

In Figure 8, we show our results for TIP4P/ICE. In Figure 8A, we visualize a crystal nucleus of size $n \approx 240$, where we can see clearly its hexagonal structure. In Figure 8B, we show the nucleation barrier $\Delta G(n)$ as a function of nucleus size n for $T = 230$ K. The blue line is the aCNT fit of the nucleation barrier. We find a barrier height of $50.4 k_B T$ with a statistical error of around $6 k_B T$. Previous Metadynamics simulations³⁹ found a barrier height of $52.8 k_B T$ with a similar statistical error of around $6 k_B T$. Therefore, we conclude that our Variational Umbrella Seeding result agrees well with the Metadynamics simulations.

In Figure 8C, we compare the nucleation rate J of

TIP4P/ICE as a function of supercooling, obtained with Seeding³⁸, Metadynamics³⁹, Lattice Mold^{40,44}, and our Variational Umbrella Seeding. To compute the nucleation rate from our nucleation barrier, we use the same kinetic prefactor of $J_0 = 10^{37} m^{-3} s^{-1}$ as was used in previous Seeding simulations.⁴⁵ Seeding has an uncertainty of around 5 orders of magnitude represented by the red shaded region. We observe that our result for the nucleation rate with Variational Umbrella Seeding (blue dot) agrees very well with previous results from Metadynamics³⁹ and Lattice Mold⁴⁰ simulations.

D. Summary of barriers

In Table I, we summarize our Variational Umbrella Seeding results for the nucleation barriers. Additionally, Table I presents reference results obtained with Umbrella Sampling for WCA³⁴ and mW³⁵ or metadynamics for TIP4P/ICE.³⁹ The barrier height varies from $\Delta G^c = 21 k_B T$ to $72 k_B T$, and the critical nucleus size ranges from $n_c = 72$ to 453. Across this wide variety of barriers and models, we observe that Variational Umbrella Seeding agrees well with the reference results within $2 - 3 k_B T$ in all cases. In general, we obtain slightly lower values for the barrier height. Both the *NPT* and the *NVE* integrator schemes give accurate results, indicating that they can both be used to obtain approximations of the barrier height.

E. Comparison with existing methods

Now that we have demonstrated that Variational Umbrella Seeding successfully reproduces nucleation barriers obtained by Umbrella Sampling and metadynamics, it is useful to discuss the advantages of Variational Umbrella Seeding compared to these and other existing methods. In short, we argue that Variational Umbrella Seeding is faster than rigorous methods, while being more accurate than Seeding.

Firstly, we have shown that Variational Umbrella Seeding is independent of the choice of order parameter. We have already discussed how this improves upon the original Seeding approach, but this argument also applies to other methods such as the nucleus size pinning method²⁰ and the persistent embryo approach,⁴⁶ since these methods also rely on the CNT approximation, Equation (2).

Secondly, using the aCNT Equation (8) for the nucleation barrier reduces the problem to fitting three parameters. In standard Umbrella Sampling, one parameter must be estimated per window to stitch the windows together. Because standard Umbrella Sampling requires overlapping windows, the number of windows quickly increases with the size of the critical nucleus. In Variational Umbrella Seeding, there is no need for overlap between different windows as there is no need to stitch these together. Therefore, Variational Umbrella Seeding only requires four windows, independent of the critical nucleus size, much less than standard Umbrella Sampling. This advantage of Variational Umbrella Seeding with respect

to standard Umbrella Sampling will be more pronounced for smaller supersaturations and larger critical nucleus sizes.

We expect that the choice of order parameter will also influence the efficiency of the CNT-US method by Russo, Romano, and Tanaka³⁵ and the method of McCarty *et al.*⁴⁷ Both of these methods rely on a bias potential of the CNT form, Equation (6a). We have seen, for example in Figure 2, that this CNT approximation can be less appropriate, especially for the initial part of the barrier. This may be problematic in the initial part of the barrier where it is very steep. In these higher gradient regions, stronger biases are needed, resulting in lower acceptance ratios for Monte Carlo schemes. This decreases the efficiency of biased simulations. In contrast, in Variational Umbrella Seeding, there is no need to perform biased simulations of the initial part of the barrier. The metastable liquid is simulated without any bias, and all the biased simulations are performed at higher nucleus sizes, where the gradient of the nucleation barrier is less steep.

An advantage with respect to metadynamics is that there is no need to compute bias forces in Variational Umbrella Seeding. This advantage has several aspects. Firstly, this makes the choice of order parameter much more flexible. In Variational Umbrella Seeding, the order parameter does not need to be differentiable. For instance, when the number of particles in the nucleus is employed as an order parameter, the order parameter takes only integer values. Therefore, the bias potential is not a continuous function of the order parameter and one cannot compute the derivative that is needed to evaluate the force. Even when order parameters are differentiable, it can be inconvenient or computationally expensive to calculate their derivatives. Secondly, order parameters do not have to be computed for every simulation timestep. Depending on the complexity of the model and the order parameter, this can lead to a significant speedup. Thirdly, Variational Umbrella Seeding is compatible with conventional molecular dynamics or Monte Carlo codes by coupling them to an external hybrid Monte Carlo scheme. There is no need to modify the molecular dynamics or Monte Carlo codes themselves, eliminating the need to ‘patch’ a program with additional software such as PLUMED.⁴⁸

For a quantitative comparison, we can compare the simulation time required to estimate the nucleation rate of TIP4P/ICE at 230K. Seeding simulations required around 1.5×10^5 central processing unit (CPU) hours.⁴⁵ With Lattice Mold simulations, this increased to around 1×10^6 CPU hours.⁵ Forward flux sampling calculations needed approximately 2×10^7 CPU hours.⁴⁹ For our Variational Umbrella Seeding simulations we used around 2×10^5 CPU hours. This comparison suggests that Variational Umbrella Seeding is more efficient than Lattice Mold, significantly more efficient than forward flux sampling, and only slightly less efficient than Seeding.

V. CONCLUSION

In conclusion, we introduced Variational Umbrella Seeding, a novel computational technique for estimating nucle-

Label	Model	T	Order parameter	n_c	$ \Delta\mu $	$n_c \Delta\mu /2$	$\Delta G^c / k_B T$		Reference
							VUS		
							NPT	NVE	
I	WCA	$0.025 \, \varepsilon/k_B$	$\xi_c = 6$	203	0.41^{34}	41.6	30.2	30.7	32.5^{34}
II	WCA	$0.025 \, \varepsilon/k_B$	$\xi_c = 7$	170	0.41^{34}	34.9	30.3	30.5	32.5^{34}
III	WCA	$0.025 \, \varepsilon/k_B$	$\xi_c = 8$	147	0.41^{34}	30.1	29.8	30.8	32.5^{34}
IV	mW	215.1 K	$\tilde{q}_6^c = 0.391$	72	0.62^{45}	22.3	21.0	21.7	23.5^{35}
V	mW	225.0 K	$\tilde{q}_6^c = 0.386$	148	0.50^{45}	37.0	38.8	38.5	40.1^{35}
VI	mW	235.0 K	$\tilde{q}_6^c = 0.380$	336	0.38^{45}	63.8	71.8	72.6	72.0^{35}
VII	TIP4P/ICE	230.0 K	$\tilde{q}_6^c = 0.378$	453	0.32^{38}	72.5	50.4	-	52.8^{39}

TABLE I. Results from Variational Umbrella Seeding (VUS) for the nucleation barriers $\Delta G^c/k_B T$ of nearly hard spheres (WCA), a monatomic model of water (mW), and the TIP4P/ICE model of water are compared with reference results from Umbrella Sampling for WCA³⁴ and mW,³⁵ or metadynamics for TIP4P/ICE.³⁹ For WCA, the pressure $P\sigma^3/k_B T = 12.0$ and the temperature $T = 0.025 \epsilon/k_B$ are fixed, while varying the order parameter for identifying the crystal nucleus, leading to different critical nucleus sizes n_c and therefore different Classical Nucleation Theory (CNT) approximations $\Delta G_{\text{CNT}}^c = n_c|\Delta\mu|/2$. For mW and TIP4P/ICE, the temperature T is varied, but the order parameter threshold is fixed using the mislabeling technique. The pressure is 0 and 1 bar, respectively, for mW and TIP4P/ICE. The barriers $\Delta G^c/k_B T$ shown in the Variational Umbrella Seeding (VUS) and Reference columns were all measured in the NPT ensemble. For Variational Umbrella Seeding, we explore two different choices for the integrator in our hybrid Monte Carlo / molecular dynamics scheme: the approximate NPT and the rigorous NVE integrator. All values shown in the columns from ‘ $|\Delta\mu|$ ’ to ‘Reference’ are in units of $k_B T$. The statistical error in n_c is around 5 particles for WCA and mW, and around 60 particles for TIP4P/ICE. The statistical error in our VUS barriers is around $0.5 k_B T$ for WCA and mW, and around $6 k_B T$ for TIP4P/ICE.

ation barriers. The theoretical basis of this method is adjusted classical nucleation theory. Hybrid molecular dynamics - Monte Carlo simulations are used to obtain segments of the nucleation barrier. We then fit the free parameters in the adjusted classical nucleation theory using a variational approach. Our results demonstrate good agreement with previous methods for estimating crystal nucleation barriers of nearly hard spheres (WCA), monatomic water (mW), and the TIP4P/ICE model of water. The nucleation barrier values ranged from $20 k_B T$ to $72 k_B T$. Variational Umbrella Seeding matched all these previous results within $3 k_B T$, which is the typical uncertainty range for these calculations.

Given its low computational cost, we believe that Variational Umbrella Seeding can serve as a valuable tool for investigating nucleation rates across wide ranges of temperatures, pressures, and particle interactions. Moreover, we anticipate that this technique can be extended to explore other nucleation processes such as condensation, cavitation, and melting.

SUPPLEMENTARY MATERIAL

Please see the supplementary material for the code used to generate and analyze the results of this paper.

ACKNOWLEDGMENTS

M.D. and W.G. acknowledge funding from the European Research Council (ERC) under the European Union’s Horizon 2020 research and innovation programme (Grant agreement No. ERC-2019-ADG 884902 SoftML). J.R.E. acknowledges funding from the Ramon Y Cajal fellowship (RYC2021-

030937-I) and the Spanish National Agency for Research (PID2022-136919-NAC33). E.S and C.V acknowledge funding from MEC by grant PID2022-136919NB-C31.

DATA AVAILABILITY STATEMENT

The data that supports the findings of this study are available within the article and its supplementary material.

Appendix A: Code

The code used to generate and analyze the results of this paper is freely available at github.com/MarjoleinDijkstraGroupUU/VariationalUmbrellaSeeding and in the supplementary material of this paper. The implementation is based on the hybrid Monte Carlo code by Guo, Haji-Akbari, and Palmer²⁷ and uses the LAMMPS code for molecular dynamics²⁹ and the freud library for calculating bond order parameters.⁵⁰

Appendix B: Barriers and fitting parameters

In Table II, we present the values of the parameters of the aCNT expression, Equation (8b), that we use to fit the nucleation barriers of WCA, mW, and TIP4P/ICE.

Label	Model	$ \Delta\mu $	g_2		g_1		g_0	
			NPT	NVE	NPT	NVE	NPT	NVE
I	WCA	0.41^{34}	4.32	4.31	-8.35	-8.21	13.46	13.22
II	WCA	0.41^{34}	3.92	3.90	-5.56	-5.33	10.51	10.21
III	WCA	0.41^{34}	3.64	3.50	-3.91	-2.75	9.39	7.99
IV	mW	0.62^{45}	4.29	4.25	-3.47	-2.98	6.15	5.43
V	mW	0.50^{45}	3.95	3.99	-0.06	-0.45	2.22	2.74
VI	mW	0.38^{45}	3.77	3.77	2.69	2.75	-1.23	-1.32
VII	TIP4P/ICE	0.32^{38}	4.32	-	-9.89	-	16.02	-

TABLE II. Fitting parameters of the aCNT expression given by Equation (8b) for the nucleation barriers of WCA, mW, and TIP4P/ICE. The labels correspond to the labels shown in Table I. The values for the supersaturation $|\Delta\mu|$ are from Refs. 34, 45, and 38 for WCA, mW, and TIP4P/ICE, respectively. All values are shown in units of $k_B T$.

Appendix C: Confidence interval

In addition to obtaining a maximum-likelihood estimate for the nucleation barrier ΔG^c , we can compute a confidence interval for the critical nucleus size and the barrier height using the likelihood function, Equation (17). To do this, we follow the procedure outlined in Ref. 51. To determine an approximate 95% confidence interval for the nucleation barrier ΔG^c , we vary the parameters $\hat{g}_2 + dg_2$ and $\hat{g}_1 + dg_1$ and compute the likelihood L relative to the likelihood of the maximum likelihood estimate, i.e. $L_{\text{rel}} = L(\hat{g}_2 + dg_2, \hat{g}_1 + dg_1) / L(\hat{g}_2, \hat{g}_1)$. The values dg_2, dg_1 for which this relative likelihood $L_{\text{rel}} = 0.05$ represent the boundaries of the 95% confidence region. Note that this criterion is specific to our case of two parameters, and a different threshold should be used to convert the relative likelihood to a confidence region if a different number of parameters is estimated. Once the boundaries of the confidence region are estimated, we can determine the critical nucleus size n_c and barrier height ΔG^c for all values of g_2 and g_1 within the 95% confidence region. In this way, we also obtain a 95% confidence interval for n_c and ΔG^c . Although these confidence intervals should always be treated with care, they can provide insights into the minimum simulation time needed to fit the aCNT parameters.

Appendix D: Optimizing fitting strategies with an idealized nucleation barrier

To optimize our fitting strategy, we performed tests with an idealized nucleation barrier. To be more precise, we assumed an idealized nucleation barrier $\Delta G(n)$ that is exactly described by the aCNT with exactly known parameter values g_i . That is, we selected values for g_i and constructed $\Delta G(n)$ accordingly. Recall that both the nucleation barrier and the external bias potential U_{ext} induce a probability distribution $p(n)$ for the nucleus size, given by

$$p(n) = \frac{1}{Z} \exp[-(\Delta G_{\text{aCNT}}(n) + U_{\text{ext}}(n))/k_B T]. \quad (\text{D1})$$

Therefore, we can numerically generate independent samples from this probability distribution, akin to conducting a biased simulation. Subsequently, we employed our maximum-likelihood approach to test how well we can recover our idealized nucleation barrier using a limited number of independent samples.

Constructing and fitting an idealized nucleation barrier in this way is relatively quick. We iteratively constructed and fitted nucleation barriers of varying heights using different fitting strategies. In this manner, we optimized the fitting strategy that we used for our simulations.

Firstly, we roughly estimate the critical nucleus size n_c . This can be efficiently obtained using the seeding technique or estimated from previous literature. We use four different windows, positioned at target sizes $\hat{n} = n_c/4, n_c/2, 3n_c/4$, and n_c . From the critical nucleus size estimate n_c , we can calculate a first estimate of the interfacial tension γ . This is enough to have an idea of the nucleation barrier using Equation (7a). From Equation (7a), we approximate the local curvature of the nucleation barrier. In order to constrain the nucleus size, the spring constant should be larger than the local curvature. To be on the safe side, the spring constant k of the bias potential is chosen to be six times⁵² the local curvature i.e.

$$k(\hat{n}) = 6 \left. \frac{d^2 \Delta G_{\text{CNT}}}{dn^2} \right|_{\hat{n}}.$$

This means that a different spring constant k is chosen for each target size \hat{n} . The idea to base the spring constant on the curvature is from Ref. 52.

¹R. J. Allen, P. B. Warren, and P. R. ten Wolde, Phys. Rev. Lett. **94**, 018104 (2005).

²P. G. Bolhuis, D. Chandler, C. Dellago, and P. L. Geissler, Annu. Rev. Phys. Chem. **53**, 291 (2002).

³A. Laio and M. Parrinello, Proc. Natl. Acad. Sci. U.S.A. **99**, 12562 (2002).

⁴F. Trudu, D. Donadio, and M. Parrinello, Phys. Rev. Lett. **97**, 105701 (2006).

⁵J. R. Espinosa, P. Sampedro, C. Valeriani, C. Vega, and E. Sanz, Faraday Discuss. **195**, 569 (2016).

⁶S. Auer and D. Frenkel, Nature **409**, 1020 (2001).

⁷G. M. Torrie and J. P. Valleau, J. Comput. Phys. **23**, 187 (1977).

⁸M. Volmer and I. Weber, Z Phys Chem **119U**, 277 (1926).

⁹R. Becker and W. Döring, Ann. Phys. **416**, 719 (1935).

¹⁰J. R. Espinosa, C. Vega, C. Valeriani, and E. Sanz, J. Chem. Phys. **144**, 034501 (2016).

- ¹¹P. Montero de Hijes and C. Vega, *J. Chem. Phys.* **156**, 014505 (2022).
- ¹²W. Gispen, G. M. Coli, R. van Damme, C. P. Royall, and M. Dijkstra, *ACS nano* **17**, 8807 (2023).
- ¹³W. Gispen and M. Dijkstra, *Phys. Rev. Lett.* **129**, 098002 (2022).
- ¹⁴B. Sadigh, L. Zepeda-Ruiz, and J. L. Belof, *Proc. Natl. Acad. Sci. U.S.A.* **118**, e2017809118 (2021).
- ¹⁵G. Fiorucci, G. M. Coli, J. T. Padding, and M. Dijkstra, *J. Chem. Phys.* **152**, 064903 (2020).
- ¹⁶T. Dasgupta, G. M. Coli, and M. Dijkstra, *ACS nano* **14**, 3957 (2020).
- ¹⁷G. M. Coli and M. Dijkstra, *ACS nano* **15**, 4335 (2021).
- ¹⁸W. Gispen and M. Dijkstra, *arXiv preprint arXiv:2401.05855* (2024).
- ¹⁹L. Filion, M. Hermes, R. Ni, and M. Dijkstra, *J. Chem. Phys.* **133**, 244115 (2010).
- ²⁰A. K. Sharma and F. A. Escobedo, *J. Chem. Phys.* **148** (2018).
- ²¹I. Sanchez-Burgos, P. M. de Hijes, P. Rosales-Pelaez, C. Vega, and E. Sanz, *Phys. Rev. E* **102**, 062609 (2020).
- ²²G. Menzl, M. A. Gonzalez, P. Geiger, F. Caupin, J. L. F. Abascal, C. Valeriani, and C. Dellago, *Proc. Natl. Acad. Sci. U.S.A.* **113**, 13582 (2016).
- ²³D. W. Oxtoby and R. Evans, *The Journal of chemical physics* **89**, 7521 (1988).
- ²⁴J. Merikanto, E. Zapadinsky, A. Lauri, and H. Vehkamäki, *Phys. Rev. Lett.* **98**, 145702 (2007).
- ²⁵S. Prestipino, A. Laio, and E. Tosatti, *Phys. Rev. Lett.* **108**, 225701 (2012).
- ²⁶M. Gonzalez, E. Sanz, C. McBride, J. L. F. Abascal, C. Vega, and C. Valeriani, *Phys. Chem. Chem. Phys.* **16**, 24913 (2014).
- ²⁷J. Guo, A. Haji-Akbari, and J. C. Palmer, *J. Theor. Comput. Chem.* **17**, 1840002 (2018).
- ²⁸F. Guidarelli Mattioli, F. Sciortino, and J. Russo, *J. Phys. Chem. B* **127**, 3894 (2023).
- ²⁹S. Plimpton, *J. Comput. Phys.* **117**, 1 (1995).
- ³⁰H. Bekker, H. Berendsen, E. Dijkstra, S. Achterop, R. v. Vondrumen, D. Vanderspoel, A. Sijbers, H. Keegstra, and M. Renardus, in *4th international conference on computational physics (PC 92)* (World Scientific Publishing, 1993) pp. 252–256.
- ³¹B. Mehlig, D. Heermann, and B. Forrest, *Phys. Rev. B* **45**, 679 (1992).
- ³²T.-S. Lee, B. K. Radak, A. Pabis, and D. M. York, *J. Chem. Theory Comput.* **9**, 153 (2013).
- ³³S. Auer and D. Frenkel, *J. Chem. Phys.* **120**, 3015 (2004).
- ³⁴L. Filion, R. Ni, D. Frenkel, and M. Dijkstra, *J. Chem. Phys.* **134**, 134901 (2011).
- ³⁵J. Russo, F. Romano, and H. Tanaka, *Nat. Mater.* **13**, 733 (2014).
- ³⁶V. Molinero and E. B. Moore, *J. Phys. Chem. B* **113**, 4008 (2009).
- ³⁷J. Russo, A. C. Â Maggs, D. Bonn, and H. Tanaka, *Soft Matter* **9**, 7369 (2013).
- ³⁸J. R. Espinosa, C. Navarro, E. Sanz, C. Valeriani, and C. Vega, *J. Chem. Phys.* **145** (2016).
- ³⁹H. Niu, Y. I. Yang, and M. Parrinello, *Phys. Rev. Lett.* **122**, 245501 (2019).
- ⁴⁰I. Sanchez-Burgos, A. R. Tejedor, C. Vega, M. M. Conde, E. Sanz, J. Ramirez, and J. R. Espinosa, *J. Chem. Phys.* **157** (2022).
- ⁴¹C. Vega, E. Sanz, and J. Abascal, *The Journal of chemical physics* **122** (2005).
- ⁴²R. W. Hockney and J. W. Eastwood, *Computer simulation using particles* (crc Press, 2021).
- ⁴³J.-P. Ryckaert, G. Ciccotti, and H. J. Berendsen, *J. Comput. Phys.* **23**, 327 (1977).
- ⁴⁴A. R. Tejedor, I. Sanchez-Burgos, E. Sanz, C. Vega, F. J. Blas, R. Davidchack, N. di Pasquale, J. Ramirez, and J. R. Espinosa, *J. Open Source Softw.* (In press).
- ⁴⁵J. R. Espinosa, E. Sanz, C. Valeriani, and C. Vega, *J. Chem. Phys.* **141** (2014).
- ⁴⁶Y. Sun, H. Song, F. Zhang, L. Yang, Z. Ye, M. I. Mendelev, C.-Z. Wang, and K.-M. Ho, *Phys. Rev. Lett.* **120**, 085703 (2018).
- ⁴⁷J. McCarty, O. Valsson, P. Tiwary, and M. Parrinello, *Phys. Rev. Lett.* **115**, 070601 (2015).
- ⁴⁸M. Bonomi, G. Bussi, C. Camilloni, G. A. Tribello, P. BanÅiÅj, A. Barducci, M. Bernetti, P. G. Bolhuis, S. Bottaro, D. Branduardi, R. Capelli, P. Carloni, M. Ceriotti, A. Cesari, H. Chen, W. Chen, F. Colizzi, S. De, M. De La Pierre, D. Donadio, V. Drobot, B. Ensing, A. L. Ferguson, M. Filizola, J. S. Fraser, H. Fu, P. Gasparotto, F. L. Gervasio, F. Giberti, A. Gil-Ley, T. Giorgino, G. T. Heller, G. M. Hocky, M. Iannuzzi, M. Invernizzi, K. E. Jelfs, A. Jussupow, E. Kirilin, A. Laio, V. Limongelli, K. Lindorff-Larsen, T. LÄjhr, F. Marinelli, L. Martin-Samos, M. Masetti, R. Meyer, A. Michaelides, C. Molteni, T. Morishita, M. Nava, C. Papissoni, E. Papaleo, M. Parrinello, J. Pfaendtner, P. Piaggi, G. Piccini, A. Pietropaolo, F. Pietrucci, S. Pipolo, D. Provasi, D. Quigley, P. Raiteri, S. Raniolo, J. Rydzewski, M. Salvalaglio, G. C. Sosso, V. Spiwok, J. Å poner, D. W. H. Swenson, P. Tiwary, O. Valsson, M. Vendruscolo, G. A. Voth, A. White, and The PLUMED consortium, *Nat. Methods* **16**, 670 (2019).
- ⁴⁹A. Haji-Akbari and P. G. Debenedetti, *Proc. Natl. Acad. Sci. U.S.A.* **112**, 10582 (2015).
- ⁵⁰V. Ramasubramani, B. D. Dice, E. S. Harper, M. P. Spellings, J. A. Anderson, and S. C. Glotzer, *Comput. Phys. Commun.* **254**, 107275 (2020).
- ⁵¹D. J. Venzon and S. H. Moolgavkar, *J. R. Stat. Soc., C: Appl. Stat.* **37**, 87 (1988).
- ⁵²J. Kästner and W. Thiel, *J. Chem. Phys.* **123** (2005).